Applied Physics Letters

RESEARCH ARTICLE | APRIL 17 2026

Carbon-doped quasi-bulk hexagonal boron nitride grown by HVPE

Z. Alemoush ; M. Almohammad ; J. Li ; J. Y. Lin ; H. X. Jiang

Appl. Phys. Lett. 128, 152106 (2026)
https://doi.org/10.1063/5.0326417

Applied Physics Letters ARTICLE pubs.aip.org/aip/apl

Carbon-doped quasi-bulk hexagonal boron nitride grown by HVPE

Cite as: Appl. Phys. Lett. **128**, 152106 (2026); doi: 10.1063/5.0326417
Submitted: 5 February 2026 · Accepted: 31 March 2026 ·
Published Online: 17 April 2026

Z. Alemoush,[a] M. Almohammad, J. Li, J. Y. Lin, and H. X. Jiang

AFFILIATIONS

Department of Electrical and Computer Engineering, Texas Tech University, Lubbock, Texas 79409, USA

[a]Author to whom correspondence should be addressed: zalemous@ttu.edu

ABSTRACT

We report characterization of 4-in. diameter carbon-doped hexagonal boron nitride (h-BN:C) quasi-bulk crystals (100 μm in thickness) produced by hydride vapor-phase epitaxy. X-ray diffraction characterization results revealed that carbon incorporation enhances crystalline quality due to carbon's role in mitigating native defect formation by substituting on both the B and N sites. Photoluminescence spectroscopy demonstrated that carbon doping fundamentally alters the optical properties. While the undoped wafer exhibits a broad emission line near 3.41 eV, the carbon-doped sample displays three distinct ultraviolet lines at 4.10, 3.91, and 3.74 eV. These peaks correspond to the zero-phonon line of a carbon defect quantum emitter and its associated phonon replicas, characterized by a room-temperature radiative lifetime of approximately 0.5 ns. Although carbon is unsuitable for conventional *n*- or *p*-type doping in h-BN, carbon doping appears to be a useful tool for improving crystalline quality and enabling the control of unique properties essential for high-efficiency neutron detectors, optoelectronics, and quantum technologies.

III-nitride wide and ultrawide bandgap (UWBG) semiconductors have attracted significant interest due to their diverse applications, ranging from LEDs for lighting, micro-LED displays/TVs, power electronics, and emerging quantum technologies.[1–3] Within this family, hexagonal boron nitride (h-BN) stands out due to its distinct layered structure and UWBG (~6 eV), which imparts unique physical and chemical attributes, including high lateral thermal conductivity, excellent dielectric strength, chemical inertness, and exceptional mechanical robustness.[4–8] Furthermore, h-BN exhibits significant potential for solid-state neutron detectors due to an unusually large thermal neutron capture cross section of the isotope boron-10 (~3840 barns).[9,10] While bulk crystal growth techniques utilizing high-pressure high-temperature (HPHT)[5,7,8,11] and metal flux solutions[12] are established, they are inherently limited. These methods typically yield only millimeter-sized crystals, offering poor prospects for wafer-scale expansion or precise doping control. However, the development of thick, large-scale h-BN wafers is a fundamental prerequisite for advanced device integration. For instance, high-sensitivity neutron detectors require both significant thickness and large surface areas to maximize the active detection volume.[13–18] To date, the only demonstrated capability for producing large-diameter, freestanding thick h-BN wafers has been reported by our group via hydride vapor-phase epitaxy (HVPE) technique.[13–18]

HVPE has previously been the gold standard for producing GaN quasi-bulk wafers due to its unique combination of high growth rates, superior control of impurity incorporation, and ability to scale to larger-diameter wafer production.[19] Our recent studies successfully leveraged HVPE to grow millimeter-thick h-BN wafers.[13–18] Detectors fabricated from these quasi-bulk layers have set new benchmarks in the field, achieving record-high detection efficiencies with 60% efficiency for thermal neutrons and 5% efficiency for 14.1 MeV fast neutrons.[13–18]

In parallel, understanding and controlling impurity incorporation, especially carbon (C) impurities, is important for advancing h-BN materials and novel devices. Carbon is inherently prevalent in III-nitride growth environments and significantly influences the electronic and optical properties of GaN and AlN by introducing both donor- and acceptor-type of impurities.[20–22] Previous studies on h-BN thin films grown by metalorganic chemical vapor deposition (MOCVD) revealed that carbon atoms substitute on both boron (C_B) as deep donors and nitrogen (C_N) as deep acceptors. These carbon-related impurities affect both optical (optical absorption and emission) and electrical properties.[23–25] First-principles calculations and recent experimental studies have demonstrated the existence of carbon in three configurations of C_B, C_N, and an interstitial form C_i with corresponding energy levels of 3.71, 3.19, and 2.40 eV above the valence band maximum (VBM), respectively.[24,25] Additionally, sharp emission lines in the UV and visible ranges, attributed to quantum emitters associated with carbon-related defect complexes, have been

reported in single- or few-layer h-BN flakes.[26–33] These features show potential applications for room-temperature quantum emitters. Despite these findings, comprehensive experimental investigations into the properties of carbon-related impurities in quasi-bulk h-BN wafers remain limited, and further studies are necessary to evaluate their implications for the material crystalline quality, optical properties, conductivity control, and device performance.

In this work, we report on the growth of carbon-doped h-BN quasi-bulk wafers by the HVPE method. Structural analysis by x-ray diffraction (XRD) demonstrated enhanced crystalline quality. Optical characterization using ultraviolet–visible (UV–Vis) absorption and photoluminescence (PL) spectroscopy revealed significant modifications introduced by carbon incorporation, including a pronounced ultraviolet emission line at 4.10 eV and its sidebands at 3.91 and 3.74 eV, which have been previously identified by many groups to be a carbon defect complex-related quantum emitter and its associated phonon replicas.[32–34] The present and previous results highlight the viability of HVPE for producing high-quality, impurity-controlled quasi-bulk h-BN wafers and provide critical insights for advancing the utilization of h-BN UWBG semiconductor technologies for electronics, photonics, neutron detectors, and quantum emitters.

HVPE growth was conducted on 4-in. diameter c-plane sapphire (Al_2O_3) substrates. Boron trichloride (BCl_3) and ammonia (NH_3) served as the boron and nitrogen precursors, respectively, delivered by nitrogen (N_2) carrier gas. A thin 30 nm low temperature h-BN buffer layer was first deposited on sapphire at 1300 °C. The growth temperature for both undoped (h-BN) and C-doped (h-BN:C) samples was 1500 °C and the growth pressure was 20 Torr. We employed *in situ* doping using methane (CH_4) gas source. The carbon concentration can be controlled precisely by a mass flow controller and is proportional to the CH_4 flow rate. At these growth conditions, the growth rate is about 25 μm per hour for both h-BN and h-BN:C samples, as confirmed by thickness profilometer measurements. The targeted sample thickness was 100 μm. After growth, h-BN and h-BN:C wafers self-delaminated from the substrate upon cooling, forming freestanding wafers due primarily to the layered crystalline structure of h-BN.[13–18] These h-BN:C freestanding samples, along with reference undoped h-BN wafers of the same thickness, were used for comparative characterization.

Figure 1 shows the carbon concentration profile probed by secondary ion mass spectrometry (SIMS) measurements for the h-BN:C wafer grown using a CH_4 flow rate of 90 sccm, revealing a carbon concentration of 5.5×10^{20} cm^{-3}. SIMS profiles were probed from either the top or bottom surface, yielding identical carbon concentration and confirming a uniform doping concentration across the entire 100 μm thickness. The inset compares the optical images of 4″-diameter freestanding undoped (h-BN) and carbon-doped (h-BN:C) wafers. The wafers exhibit smooth surfaces across the entire area, with no visible cracks. A strong yellow color is observed in the h-BN:C wafer, while the undoped h-BN wafer is transparent. The results suggest that carbon impurities tend to introduce mid-gap absorption. Such coloration and sub-bandgap absorption are consistent with the expectation that carbon doping tends to introduce deep impurity levels in h-BN, analogous to the well-known "yellow luminescence" in GaN commonly associated with carbon-related deep acceptor states.[20,22]

We first performed ultraviolet–visible (UV–Vis) absorption spectroscopy on h-BN and h-BN:C wafers to assess the overall impact

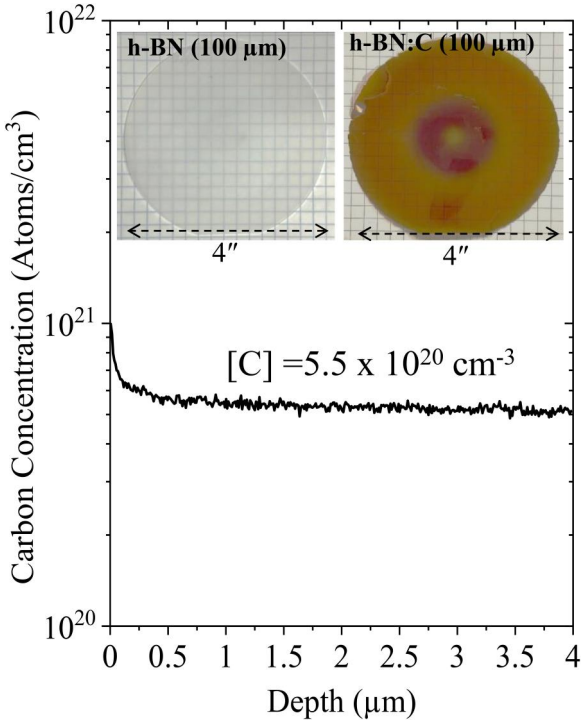

FIG. 1. Carbon doping profile in carbon-doped (h-BN:C) wafer grown using a CH_4 flow rate of 90 sccm, probed by secondary ion mass spectrometry (SIMS). A uniform carbon concentration of approximately 5.5×10^{20} cm^{-3} is observed. Inset shows optical images of whole 4″-diameter freestanding wafers of undoped (h-BN) and carbon-doped (h-BN:C) samples after delamination from sapphire substrate.

of carbon impurities on the optical properties. As shown in Fig. 2, the undoped wafer exhibits a sharp absorption onset near 200 nm, corresponding to the intrinsic band edge absorption of h-BN, and remains transparent across the visible spectrum, a hallmark of a high-purity UWBG semiconductor material. In contrast, below bandgap absorption bands extending into 250–400 nm are clearly seen in the h-BN:C wafer, which imparts a notable yellow tint to the material. Blue and green light are absorbed, while longer wavelengths are transmitted, resulting in the material's strong yellowish appearance.[22] This behavior mirrors the role of carbon in other III-N semiconductors (e.g., GaN), where carbon impurities create deep impurity states that lead to strong mid-gap absorption and characteristic luminescence.[20] To gain insight into how carbon atoms substitute into the BN lattice, x-ray photoelectron spectroscopy (XPS) measurements were conducted. The inset of Fig. 2 displays the XPS spectrum of the C 1s core level measured for the h-BN:C sample (red dots). The experimental data were fitted using a Gaussian–Lorentzian function, revealing a primary peak (black circles) centered at 284.8 eV, characteristic of hybridized C–C bonding (graphitic carbon). Two additional components were resolved: a lower-energy peak at 283.3 eV (purple dots) corresponding to C–B bonds, and a higher-energy peak at 286.0 eV (blue squares) attributed to C–N bonds.[35–37] These chemical shifts and the resulting bonding analysis confirm that C atoms substitute on both B and N sites and that B, N, and C atoms bond with one another,

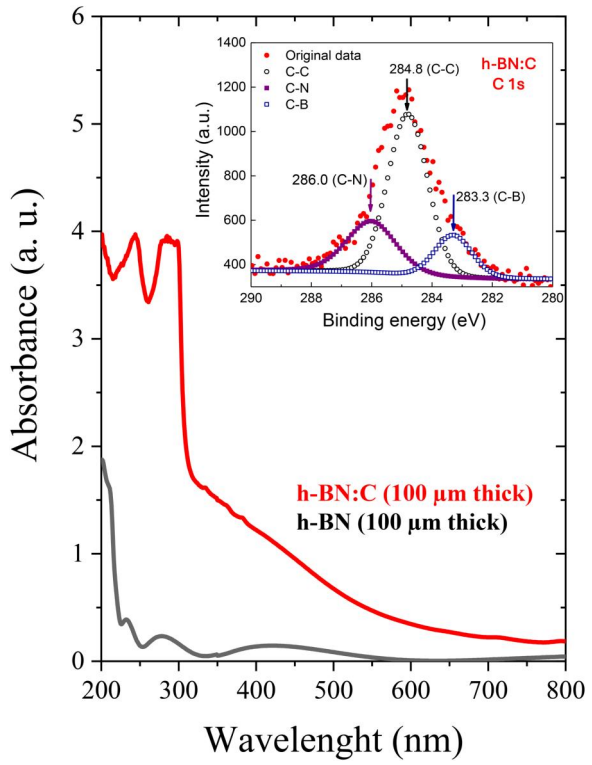

FIG. 2. UV–Vis absorbance spectra of undoped (h-BN, black curve) and carbon-doped (h-BN:C red curve) wafers grown by HVPE. The h-BN:C wafer shows stronger absorption between 250 and 500 nm wavelengths, resulting in the yellowish appearance. The inset shows an XPS spectrum of C 1s core level measured for h-BN:C sample.

and mix atomically within the lattice. This is partly because C atoms tend to incorporate into h-BN as C–C pairs.[31] Indeed, by employing aberration-corrected scanning transmission electron microscopy (STEM) on monolayer h-BN, a previous study provided direct imaging results identifying C substituting for B as well as for N.[38] Future TEM and STEM analyses will be valuable to further identify the nature of carbon substitution within the BN lattice and any potential elemental segregation or inhomogeneities in h-BN:C quasi-bulk crystals.

The growth of quasi-bulk h-BN with high crystalline quality presents considerable challenges due to the strong pre-reaction between B and N precursors at high temperatures, which leads to parasitic gas-phase reactions, leading to the formation of B–N clusters that consume the reactive precursors and promote undesirable nucleation, thereby reducing the growth rate and crystalline quality of the material.[16] However, the results shown in Fig. 3 indicate that carbon doping results in a significant improvement in crystalline quality. Figure 3(a) presents the x-ray diffraction (XRD) θ–2θ scans of undoped (black curve) and C-doped (red curve) samples for direct comparison. In each case, a single (002) diffraction peak is observed at $2\theta = 26.74°$, corresponding to a c-axis lattice constant of 6.66 Å, consistent with phase-pure hexagonal BN. However, the C-doped sample exhibits nearly two orders of magnitude higher (002) peak intensity compared to the undoped sample. Since the two samples are of identical thickness (100 μm) and were measured under identical experimental configurations, the increase in (002) peak intensity in C-doped sample relative to the undoped sample indicates significantly improved mosaic coherence and c-axis structural order.

The XRD rocking curves (or ω-scans) shown in Fig. 3(b) indicate that the full width at half maximum (FWHM) is narrowed by approximately 100 arc sec for the C-doped sample in comparison with the undoped h-BN sample. While the FWHM differences are subtle, h-BN:C exhibits a noticeably more symmetric rocking curve.

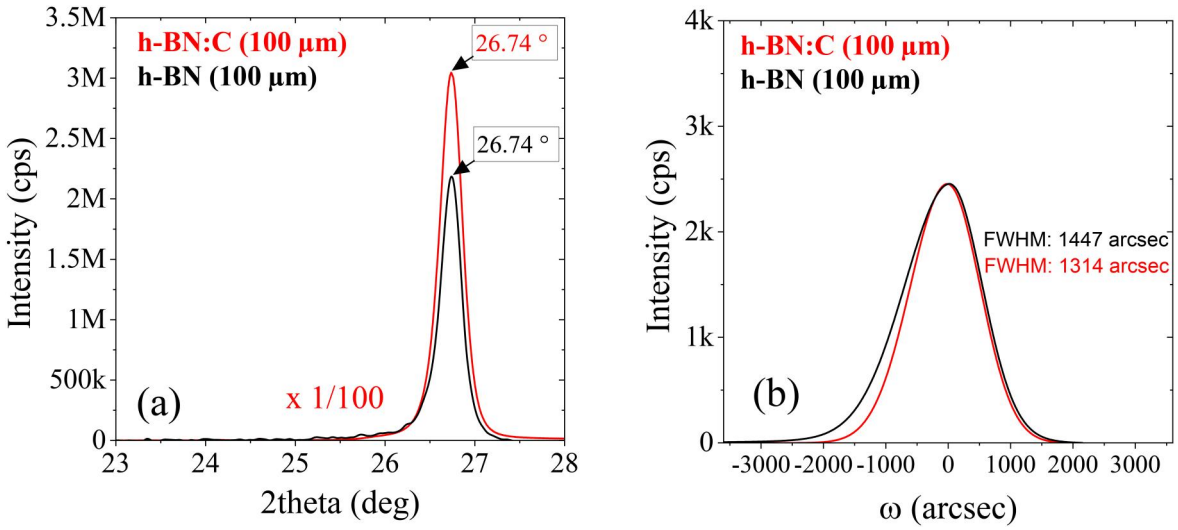

FIG. 3. XRD of undoped (h-BN, black curve) and carbon-doped (h-BN:C, red curve) samples: (a) 2θ scan of (002) peak and (b) rocking curve of (002) peak.

Since such asymmetry typically arises from vertical lattice parameter gradients, the XRD rocking curve results suggest a more uniform structural profile in the doped samples, further corroborating the findings in Fig. 3(a). We attribute this enhancement in crystalline structure of h-BN:C to carbon's role in mitigating native defect formation by substituting on both B and N sites, forming C_N and C_B, thereby reducing the number of nitrogen vacancies (V_N) and boron vacancies (V_B) and promoting a more ordered layered structure compared to the undoped baseline. The results of Fig. 3 provide several interesting insights: (1) there are nitrogen and boron vacancies in undoped h-BN wafers, (2) C tends to occupy both N and B sites, supported by the XPS results shown in the inset of Fig. 2 and also by theoretical[24] and STEM results,[38] and (3) the incorporation of C_N and C_B seems to improve the stacking order in comparison with the presence of V_N and V_B.

Regarding the electrical impact of C-doping, I–V characterization reveals that this concentration reduces electrical resistivity by nearly three orders of magnitude. However, the material remains highly resistive at approximately $\sim 10^{10}\,\Omega$ cm. The order of magnitude reduction in the electrical resistivity by C-doping is consistent with our previous observation in MOCVD grown BN-rich BNC alloy thin films.[36] The sustained high resistivity is attributed to the deep energy levels predicted for C-related impurities and defects in h-BN.[24]

Figure 4 compares the PL spectra of h-BN (black curve) and h-BN:C (red curve) samples under excitation using a pulsed excimer laser (193 nm, 20 ns pulse width, and 40 Hz repetition rate). Measurements were performed at 300 K to evaluate the effect of carbon doping on the room temperature optical emission characteristics of h-BN. As shown in Fig. 4, the PL spectrum of undoped h-BN exhibits a single dominant emission peak centered around 3.40 eV. On the other hand, the PL spectrum of the C-doped sample reveals three distinct peaks at 3.74, 3.91, and 4.10 eV. The emergence of these peaks can be attributed to the radiative recombination processes associated with carbon impurities. In fact, the 4.10 eV emission line has been attributed to quantum emitters associated with carbon dimer defects (C_BC_N).[31] The lower-energy peaks at 3.91 and 3.74 eV are typically identified as longitudinal optical (LO) phonon replicas of the 4.1 eV zero-phonon line (ZPL).[32–34]

To resolve and characterize carbon-related emission features, PL measurements were carried out on the carbon-doped sample using a frequency-quadrupled femtosecond (fs) Ti:sapphire laser ($\lambda_{exc} = 195$ nm, 6.35 eV) operating at 76 MHz at two different temperatures, as shown in Figs. 5(a) and 5(b). At 300 K in Fig. 5(a), the PL spectrum of h-BN:C reveals three distinctive peaks at 3.74, 3.91, and 4.10 eV, consistent with the structured emission observed in Fig. 4. When the temperature is lowered to 10 K as shown in Fig. 5(b), these peaks become even more pronounced and sharper with reduced spectral linewidth. The enhanced separation and narrowing of the peaks at low temperatures support the previous interpretation that these

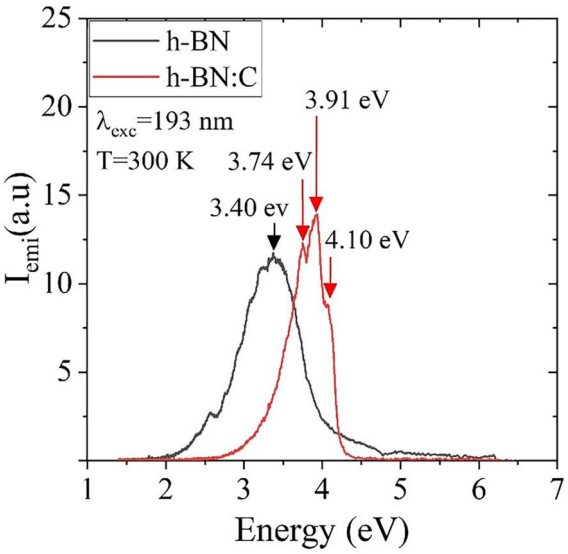

FIG. 4. Room-temperature PL spectra of undoped (h-BN) and C-doped (h-BN:C) samples under 193 nm pulsed excimer laser excitation (20 ns pulse width, 40 Hz repetition rate).

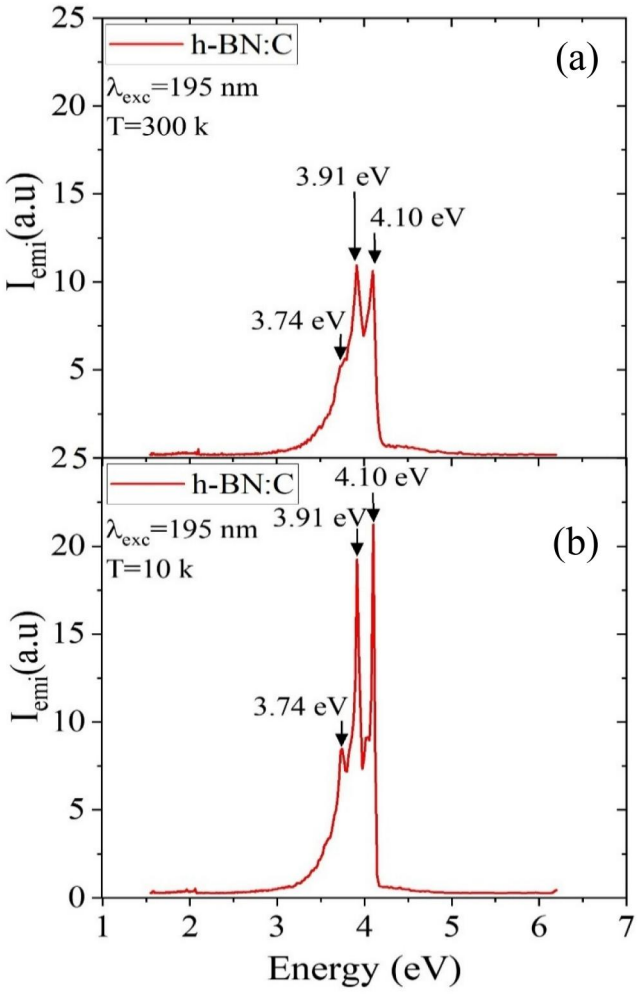

FIG. 5. PL spectra of h-BN:C measured under excitation by a frequency-quadrupled femtosecond (fs) Ti:sapphire laser ($\lambda_{exc} = 195$ nm, 6.35 eV) at (a) 300 K and (b)10 K, showing the carbon-related emission peaks at 3.74, 3.91, and 4.10 eV with enhanced sharpening/separation at low temperature.

emissions originate from discrete carbon-related defect states with well-defined transition energies,[26–33] rather than from a broad distribution of shallow or strongly phonon-broadened states. Furthermore, the peak positions of these three sharp emission lines were independent of measurement temperature, a characteristic of quantum emitters.

To further investigate the nature of these three ultraviolet emission lines observed in h-BN:C, time-resolved PL (TRPL) measurements were performed. As shown in Fig. 6, the decay curves were recorded at emission peak energies of 3.74, 3.91, and 4.10 eV. The temporal responses of the PL intensity as a function of time, I(t), were fitted by a single exponential function, $I(t) = A\exp(-t/\tau)$, where A is the initial amplitude, and τ is the characteristic decay lifetime, yielding $\tau = 0.53$, 0.52, and 0.50 ns, respectively (corresponding to an average lifetime of $\tau = 0.52 \pm 0.02$ ns). TRPL measurements provide additional insight into the recombination dynamics of the carbon-related emission lines. The fitted curves follow the experimental data closely, indicating that the radiative recombination process is dominated by a single decay channel. The nearly identical sub-nanosecond lifetimes indicates that all three peaks share a common recombination channel rather than from independent defect centers and therefore further corroborate the picture that the 4.10 eV line can be assigned to the ZPL, while the 3.91 and 3.74 eV lines correspond to its phonon sidebands.[32–34] The predicted radiative lifetime at room temperature for carbon dimer defects (C_BC_N) in h-BN is 1.2 ns,[31] in comparison to the measured lifetime of $\tau = 0.52$ ns here.

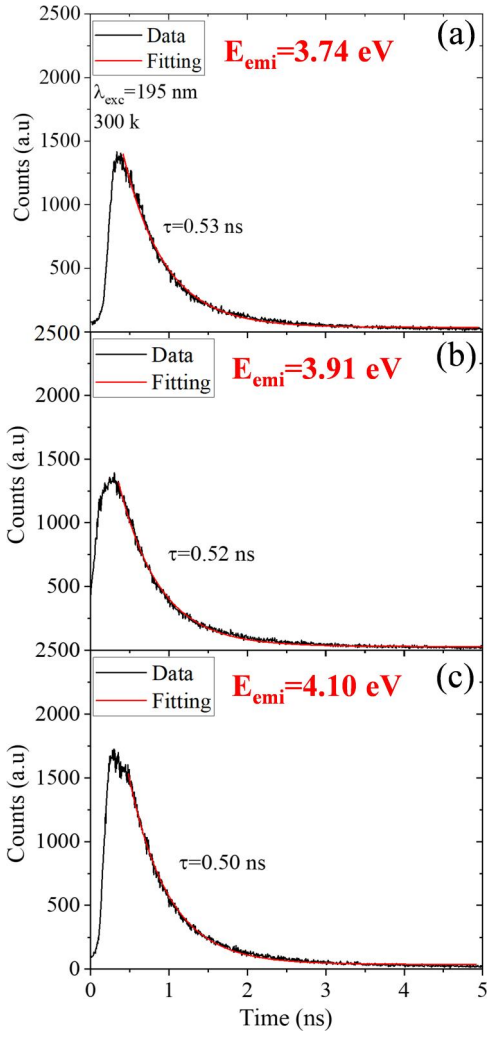

FIG. 6. Temporal responses measured at T = 300 K for emission peak energies of (a) 3.74, (b) 3.91, and (c) 4.10 eV observed in h-BN:C sample. The black lines represent experimental data, while the red lines are fitted curves using single exponential decay. The extracted lifetimes are almost identical, at 0.52 ± 0.02 ns.

It is worth noting that a pronounced 1.31 eV infrared donor–acceptor pair emission was also observed in HVPE-grown carbon-doped quasi-bulk h-BN, which was attributed to recombination between C_B donors and interstitial C_i acceptors.[25] More interestingly, it was shown that carbon defect complexes in h-BN also form quantum defects with tailored emission wavelengths within the C-band of telecom wavelength (1530–1565 nm), potentially facilitating the integration of quantum technologies into existing photonics infrastructure.[39] These findings collectively highlight the importance of controlled carbon doping to its optoelectronic properties.

In summary, we have demonstrated hydride vapor-phase epitaxy growth of quasi-bulk carbon-doped h-BN wafers (100 μm thick) 4″ in diameter. Structural characterization results revealed that carbon incorporation significantly enhances crystalline quality due to carbon's role in substituting on both the B and N sites, thereby reducing the number of boron and nitrogen vacancies. Moreover, carbon incorporation introduces pronounced mid-gap absorption and fundamentally modifies the luminescence features, where undoped h-BN's broad 3.41 eV defect line is substituted by three sharp ultraviolet PL lines at 4.10, 3.91, and 3.74 eV, previously assigned to the zero-phonon line (ZPL) of a carbon-related quantum emitter and its phonon replicas. Time-resolved PL reveals room-temperature radiative lifetimes of approximately 0.5 ns for all three lines. The present and previous results demonstrate that while carbon is unsuitable for conventional *n*- or *p*-type doping, its intentional incorporation in h-BN can effectively passivate structural defects and activate tunable quantum emitters from C-band communication wavelength to the deep UV, providing a robust avenue to tailor its optical properties. This carbon doping approach expands the functionality of h-BN for a variety of applications, including high-efficiency neutron detectors, deep-UV optoelectronics, and quantum photonic devices for single-photon generation.

The information, data, or work presented herein was funded in part by the Advanced Research Projects Agency-Energy (ARPA-E), U.S. Department of Energy, under Award No. DE-AR0001552 monitored by Dr. Olga Spahn, Dr. Jeffery Snyder, and Dr. Eric Carlson. The views and opinions of the authors expressed herein do not necessarily state or reflect those of the United States Government or any agency thereof. Jiang and Lin are grateful to the AT&T Foundation for the support of the Ed Whitacre and Linda Whitacre endowed chairs.

AUTHOR DECLARATIONS

Conflict of Interest

The authors have no conflicts to disclose.

Author Contributions

Z. Alemoush: Data curation (equal); Formal analysis (equal); Methodology (equal); Software (equal); Validation (equal); Visualization (equal); Writing – original draft (equal). **M. Almohammad:** Data curation (equal); Formal analysis (equal); Funding acquisition (equal); Software (equal); Validation (equal); Visualization (equal). **J. Li:** Data curation (equal); Formal analysis (equal); Investigation (equal); Methodology (equal); Resources (equal); Software (equal); Supervision (equal); Validation (equal); Visualization (equal). **J. Y. Lin:** Conceptualization (equal); Funding acquisition (equal); Investigation (equal); Methodology (equal); Project administration (equal); Resources (equal); Supervision (equal); Validation (equal); Writing – review & editing (equal). **H. X. Jiang:** Conceptualization (equal); Formal analysis (equal); Funding acquisition (equal); Investigation (equal); Methodology (equal); Project administration (equal); Resources (equal); Supervision (equal); Validation (equal); Visualization (equal); Writing – review & editing (equal).

DATA AVAILABILITY

The data that support the findings of this study are available within the article.

REFERENCES

[1]Nobel Prize, see NobelPrize.org for "The Nobel Prize in Physics 2014—Press Release" (2014).
[2]S. Nakamura, S. J. Pearton, and G. Fasol, *The Blue Laser Diode* (Springer, Berlin, Heidelberg, 2000).
[3]H. X. Jiang and J. Y. Lin, "How we made the microLED," Nat. Electron. **6**, 257 (2023).
[4]T. Sugino, K. Tanioka, S. Kawasaki, and J. Shirafuji, "Characterization and field emission of sulfur-doped boron nitride synthesized by plasma-assisted chemical vapor deposition," Jpn. J. Appl. Phys. **36**, L463 (1997).
[5]K. Watanabe, T. Taniguchi, and H. Kanda, "Direct-bandgap properties and evidence for ultraviolet lasing of hexagonal boron nitride single crystal," Nat. Mater. **3**, 404 (2004).
[6]B. Arnaud, S. Lebègue, P. Rabiller, and M. Alouani, "Huge excitonic effects in layered hexagonal boron nitride," Phys. Rev. Lett. **96**, 026402 (2006).
[7]Y. Kubota, K. Watanabe, O. Tsuda, and T. Taniguchi, "Deep ultraviolet light-emitting hexagonal boron nitride synthesized at atmospheric pressure," Science **317**, 932 (2007).
[8]G. Cassabois, P. Valvin, and B. Gil, "Hexagonal boron nitride is an indirect bandgap semiconductor," Nat. Photonics **10**, 262 (2016).
[9]G. F. Knoll, *Radiation Detection and Measurement*, 4th ed. (John Wiley & Sons, 2010).
[10]O. Osberghaus, "Die isotopenhäufigkeit des bors. Massenspektrometrische untersuchung der elektronenstoßprodukte von BF3 und BCl3," Z. Phys. **128**, 366 (1950).
[11]Y. Hattori, T. Taniguchi, K. Watanabe, and K. Nagashio, "Comparison of device structures for the dielectric breakdown measurement of hexagonal boron nitride," Appl. Phys. Lett. **109**, 253111 (2016).
[12]C. Yuan, J. Li, L. Lindsay, D. Cherns, J. W. Pomeroy, S. Liu, J. H. Edgar, and M. Kuball, "Modulating the thermal conductivity in hexagonal boron nitride via controlled boron isotope concentration," Commun. Phys. **2**, 43 (2019).
[13]G. Somasundaram, N. K. Hossain, Z. Alemoush, A. Tingsuwatit, J. Li, J. Y. Lin, and H. X. Jiang, "Development of millimeter-thick hexagonal boron nitride wafers and fast neutron detectors," Appl. Phys. Lett. **126**, 212104 (2025).
[14]H. X. Jiang and J. Y. Lin, "Hexagonal boron nitride: Physical properties, HVPE growth of large-diameter quasi-bulk wafers and applications," Phys. Status Solidi B **263**, e202400605 (2025).
[15]A. Tingsuwatit, A. Maity, S. J. Grenadier, J. Li, J. Y. Lin, and H. X. Jiang, "Boron nitride neutron detector with the ability for detecting both thermal and fast neutron," Appl. Phys. Lett. **120**, 232103 (2022).
[16]Z. Alemoush, M. Almohammad, J. Li, J. Y. Lin, and H. X. Jiang, "Development of 6-inch h-BN thick wafers," AIP Adv. **15**, 065003 (2025).
[17]Z. Alemoush, A. Tingsuwatit, A. Maity, J. Li, J. Y. Lin, and H. X. Jiang, "Status of h-BN quasi-bulk crystals and high efficiency neutron detectors," J. Appl. Phys. **135**, 175704 (2024).
[18]G. Somasundaram, Z. Alemoush, J. Li, J. Y. Lin, and H. X. Jiang, "Direct detection of 14.1 MeV neutrons by multi-stacked h-BN detector," Appl. Phys. Lett. **127**, 162103 (2025).
[19]R. Kucharski, T. Sochacki, B. Lucznik, and M. Bockowski, "Growth of bulk GaN crystals," J. Appl. Phys. **128**, 050902 (2020).
[20]M. A. Reshchikov, "On the origin of the yellow luminescence band in GaN," Phys. Status Solidi B **260**, 2200488 (2022).
[21]M. Kneissl, T. Y. Seong, J. Han, and H. Amano, "The emergence and prospects of deep-ultraviolet light-emitting diode technologies," Nat. Photonics **13**, 233 (2019).
[22]J. L. Lyons, A. Janotti, and C. G. Van de Walle, "Carbon impurities and the yellow luminescence in GaN," Appl. Phys. Lett. **97**, 152108 (2010).
[23]M. R. Uddin, J. Li, J. Y. Lin, and H. X. Jiang, "Probing carbon impurities in hexagonal boron nitride epilayers," Appl. Phys. Lett. **110**, 182104 (2017).
[24]C. Weston, D. Wickramaratne, M. M. Li, and C. G. Van de Walle, "Native point defects and impurities in hexagonal boron nitride," Phys. Rev. B **97**, 214104 (2018).
[25]M. Almohammad, Z. Alemoush, J. Li, J. Y. Lin, and H. X. Jiang, "Carbon-related donor–acceptor pair transition in the infrared in h-BN," Appl. Phys. Lett. **124**, 102106 (2024).
[26]T. T. Tran, K. Bray, M. J. Ford, M. Toth, and I. Aharonovich, "Quantum emission from hexagonal boron nitride monolayers," Nat. Nanotechnol. **11**, 37 (2016).
[27]N. Mendelson, D. Chugh, J. R. Reimers, T. S. Cheng, A. Gottscholl, H. Long *et al.*, "Identifying carbon as the source of visible single-photon emission from hexagonal boron nitride," Nat. Mater. **20**, 321 (2021).
[28]F. Hayee, L. Yu, J. L. Zhang, C. J. Ciccarino, M. Nguyen, A. F. Marshall *et al.*, "Revealing multiple classes of stable quantum emitters in hexagonal boron nitride with correlated optical and electron microscopy," Nat. Mater. **19**, 534 (2020).
[29]M. Maciaszek, L. Razinkovas, and A. Alkauskas, "Thermodynamics of carbon point defects in hexagonal boron nitride," Phys. Rev. Mater. **6**, 014005 (2022).
[30]C. Jara, T. Rauch, S. Botti, M. A. Marques, A. Norambuena, R. Coto *et al.*, "First-principles identification of single photon emitters based on carbon clusters in hexagonal boron nitride," J. Phys. Chem. A **125**, 1325 (2021).
[31]M. Mackoit-Sinkeviciene, M. Maciaszek, C. G. Van de Walle, and A. Alkauskas, "Carbon dimer defect as a source of the 4.1 eV luminescence in hexagonal boron nitride," Appl. Phys. Lett. **115**, 212101 (2019).
[32]T. Q. P. Vuong, G. Cassabois, P. Valvin, V. Jacques, A. Van Der Lee, A. Zobelli, K. Watanabe, T. Taniguchi, and B. Gil, "Phonon-photon mapping in a color center in hexagonal boron nitride," Phys. Rev. Lett. **117**, 097402 (2016).
[33]R. Bourrellier, S. Meuret, A. Tararan, O. Stephan, M. Kociak, L. H. G. Tizei, and A. Zobelli, "Bright UV single photon emission at point defects in h-BN," Nano Lett. **16**, 4317 (2016).
[34]X. Z. Du, J. Li, J. Y. Lin, and H. X. Jiang, "The origin of deep-level impurity transitions in hexagonal boron nitride," Appl. Phys. Lett. **106**, 021110 (2015).
[35]H. Kunzli, P. Gantenbein, R. Steiner, and P. Oelhafen, "Deposition and characterization of thin boron-carbide coatings," Anal. Chem. **346**, 41 (1993).
[36]M. R. Uddin, S. Majety, J. Li, J. Y. Lin, and H. X. Jiang, "Layer-structured hexagonal (BN)C semiconductor alloys with tunable optical and electrical properties," J. Appl. Phys. **115**, 093509 (2014).
[37]E. G. Wang, "A new development in covalently bonded carbon nitride and related materials," Prog. Mater. Sci. **41**, 241 (1997).
[38]O. Krivanek, M. Chisholm, V. Nicolosi *et al.*, "Atom-by-atom structural and chemical analysis by annular dark-field electron microscopy," Nature **464**, 571 (2010).
[39]H. X. Jiang, J. Li, J. Y. Lin, M. Almohammad, and Z. Alemoush, "Methods and systems for engineering c-band telecom-wavelength quantum defects," U.S. patent WO/2025/235025 (13 November 2025), see https://patentscope.wipo.int/search/en/WO2025235025.